Biologically-Inspired Visual Landmark Learning for Mobile Robots

Giovanni Bianco and Riccardo Cassinis*

University of Brescia, Dept. of Elect. for Automation, Via Branze 38, I-25123 Brescia - Italy, {bianco,cassinis}@ing.unibs.it

Abstract. This paper presents a biologically-inspired method for selecting visual landmarks which are suitable for navigating within not pre-engineered environments. A landmark is a region of the goal image which is chosen according to its reliability measured through a phase called *Turn Back and Look (TBL)*. This mimics the learning behavior of some social insects. The TBL phase affects the conservativeness of the vector field thus allowing us to compute the visual potential function which drives the navigation to the goal. Furthermore, the conservativeness of the navigation vector field allows us to assess if the learning phase has produced good landmarks. The presence of a potential function means that classical control theory principles based on the Liapunov functions can be applied to assess the robustness of the navigation strategy. Results of experiments using a *Nomad200* mobile robot and a color camera are presented throughout the paper.

1 Introduction

Animals, including insects, are proficient in navigating and, in general, several biological ways of solving navigational tasks seem to be promising for robotics applications. The different methods of navigating have been recently studied and categorized as (Trullier et al., 1997): *guidance, place recognition - triggered response, topological* and *metric* navigations. In order to perform such tasks animals usually deal with identifiable objects in the environment called *landmarks* (Wehner, 1992).

The use of landmarks in robotics has been extensively studied (Borenstein et al., 1996; Thrun, 1996). Basically, a landmark needs to possess characteristics such as the *stationarity*, *reliability* in recognition, and *uniqueness*. These properties must be matched with the nature of a landmark: landmarks can be *artificial* or *natural*. Of course it is much easier to deal with artificial landmarks instead of dealing with natural ones, but the latter is more appealing because their use requires no engineering of the environment. However, a general method of

dealing with natural landmarks still remains to be introduced. The main problem lies in the selection of the most suitable landmarks (Mori et al., 1995; Thrun, 1996).

Recently it has been discovered that wasps and bees perform specific flights during the first journeys to a new place to learn color, shape and distance of landmarks. Those flights are termed *Turn Back and Look (TBL)* (Lehrer, 1993). Once the place has been recognized using landmarks, insects can then accomplish navigation actions accordingly. The Cartwright and Collett model (Cartwright and Collett, 1983) is one of the main methods of navigating (Trullier et al., 1997).

The aim of this paper is to show the learning system of a biologically-inspired navigation method based on natural visual landmarks. The introduced system will select natural landmarks from the environment adopting the TBL phase (section 2).

From the selected landmarks suitable navigation movements will be computed (section 3) and in section 4 the guidance principle and how this can be influenced by the TBL phase will be addressed. The

measurable effects of TBL (namely, the *conservativeness* of the navigation vector field) is a way to assess the quality of the landmarks chosen by the learning phase.

The conservativeness of the field also permits to compute the (unique) potential function which drives landmark navigations and formal ways to assess the robustness of the whole approach can be introduced. In fact, the presence of a potential function around the goal is a sufficient condition for the application of the classical control theory based on Liapunov functions. Tests performed with the *Nomad200* will conclude the paper (section 5).

2   Learning Landmarks

A landmark must be reliable for accomplishing a task and landmarks which appear to be appropriate for human beings are not necessarily appropriate for robots because of the completely different sensor apparatus and matching systems (Thrun, 1996).

For example, the necessity of performing specific learning flights allows the insects to deal with objects which protroud from the background or which lie on a different plane than the background (Collett and Zeil, 1996). Attempts to understand in detail the significance of learning flights have been made only recently. Essentially, the flights are invariant in certain dynamic and geometric structures thus allowing the insects to artificially produce visual cues in specific areas of the eyes (Zeil et al., 1996). Perhaps, the main reason is that the precision for the homing mostly depends upon the proximity of chosen landmarks to the goal (Cheng et al., 1987). In fact, those flights need to be repeated whenever some changes in the goal position occur (Lehrer, 1997). Therefore, it becomes crucial to understand whether or not a landmark is robust for the task accomplished by the agent.

Following the biological background and reconsidering the results presented in (Thrun, 1996), one key point is that once the meaning of reliability has been established then the problem of selecting landmarks is automatically solved. Therefore, stating what is meant by *reliability of landmarks*, once given the specific sensor and matching apparatus is a mandatory step.

2.1   Sensor and matching apparatus

The use of visual landmarks asks for real-time performances and this can lead to the use of specific hardware for their identification. The robot *Nomad200* (figure 1) that was used to accomplish the tests includes the *Fujitsu Tracking Card (TRV)* which performs real-time tracking of full color templates at a NTSC frame rate (30Hz). Basically, a template is a region of a frame which can be identified by two parameters m_x and m_y representing the sizes along X and Y axes respectively.

Figure 1: The *Nomad200*

The card can simultaneously track many templates which have been previously stored in a video RAM. For each stored template the card performs a match in a sub-area of the actual video frame adopting the block matching method. This introduces the concept of *correlation* between the template and a sub-area of the actual video frame. The correlation measure is given by the sum of the absolute differences between the values of the pixels.

To track a template it is necessary to calculate the distortion between the template and a frame not only at one point on the frame but at a number of points within a *searching area*. The searching area is composed of 16×16 positions in the frame. The whole set of computed correlation measures is known by the term *correlation matrix*. Examples of correlation matrices are reported in figure 15 at the end of the paper. To perform the tracking, the matching system proposes as an output the coordinates of the position which represents the global minimum in the correlation matrix.

This approach strongly resembles the *region-based optical flow* techniques (Anandan, 1989; Little and Verri, 1989). There, the flow is defined as the shift that yields the best fit between the image regions at different times.
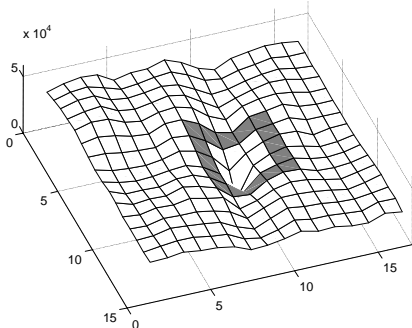
Figure 2: The neighborhood used in the *Valley Method*

2.2 Choosing the best landmarks

Mori *et al.* have taken advantage of the correlation matrix to generate attention tokens from scenes (Mori et al., 1995). The method they introduced is suitable to be used in the case of self-extraction of landmarks. Relaxing their method (the *valley method*) the following can be obtained:

$$r = 1 - \frac{g}{g'} \qquad (1)$$

where the global minimum is g and local minimum is g'. The local minimum is computed in a circle around g as visible in figure 2. The value r is a measure on how the template is uniquely identifiable in its neighborhood: the greater r the more uniquely identifiable the template. Therefore, by reliable landmarks we mean *templates which are uniquely identifiable.*

There are several degrees of freedom in searching for the best landmarks within a video frame. These are the coordinates of the origin of a landmark and its sizes along X and Y. Some simplifications can be introduced (Bianco, 1998): only squared templates are used ($m_x = m_y$), and the position of a landmark is searched for by maximizing the following:

$$(o_x^*, o_y^*) = \arg \max_{(o_x, o_y) \in \text{grid}} r_l(o_x, o_y) \qquad (2)$$

where $r_l(o_x, o_y)$ identifies the reliability factor for a landmark l whose origin is located in (o_x, o_y) representing a cross of a grid. Therefore the position (o_x^*, o_y^*) with the highest r is returned. In order to assure that different landmarks occupy different positions, previously chosen coordinates are not

considered. Examples of landmarks chosen are reported at the end of the paper in figure 16.

Once the best landmarks have been chosen from the static image of the goal, then they are stored in an internal video RAM to be used for successive tasks, the first being the Turn Back and Look.

2.3 The Turn Back and Look phase

The landmarks which have been *statically* chosen will be used for navigation tasks. We found that it was necessary to *test* them in order to verify whether they represent good guides for navigation tasks.

TBL can help in verifying this (Collett and Zeil, 1996; Bianco, 1998) by testing whether during the motion the statically chosen landmarks still remain robustly identifiable.

Through a series of stereotype movements small perturbations (local lighting conditions, changes in camera heading, different perspectives and so on) can influence the reliability of the statically chosen landmarks. Referring to figure 3, the robot goes from the top to the bottom and the camera (arrows pointing to the top) is continuously pointing towards the goal.
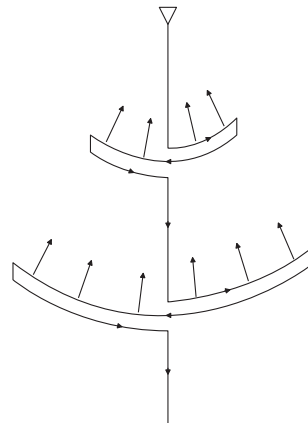

Figure 3: The arcs performed by the robot to implement the TBL phase

These sorts of perturbations occur in typical robot journeys thus allowing us to state that the TBL phase represents a *testing framework* for landmarks. In other words, the robot tries to *learn* which landmarks can be suitably used in real navigation tasks by simulating the conditions the robot will encounter along the paths.

At the end of the TBL process only those landmarks that are visible and whose reliability r_l is above a threshold are suitable to be used in navigation tasks.

The reliability factor r_l for landmark l is continuously computed during the TBL phase through the following:

$$r_l = \frac{\sum_{i=1}^{TBL} r_l^i}{TBL} \qquad (3)$$

where TBL is the total number of steps exploited till that time, and r_l^i is the reliability of landmark l calculated at time i. In the tests, at the end of the phase, TBL usually consists of 400 steps (an internal counter) and takes about 13 seconds to be performed. In figure 17, which has been reported at the end of the paper, two pictures taken by a TBL phase exploited by the robot are shown.

3 Navigation from landmarks

After reliable landmarks have been chosen then navigation information can be extracted from them (Bianco, 1998; Bianco and Zelinsky, 1999). The underlying biological principle is that a real movement is represented by an *attraction* force. It is produced by taking into account that the agent tries to restore the original position and size of the involved landmarks (Cartwright and Collett, 1983). The data can be fused together by weighing them by introducing a sigmoid function $s(r_l)$ ranging from 0 to 1. The overall navigation vector can be thus calculated as:

$$\vec{V} = [V_x \ V_y] = \frac{\sum_{l=1}^{L} \vec{v}_l \cdot s(r_l)}{\sum_{l=1}^{L} s(r_l)} \qquad (4)$$

where L is the number of landmarks chosen after TBL, r_l is the reliability value of landmark l and $\vec{v}_l$ is the attraction force *felt* by landmark l. Lastly, V_x and V_y represent an estimation of the distance (along x and y axes of the environment) from the actual position to the goal position.

Figure 4 summarizes the situation where the picture represents a typical frame taken during a navigation test. In particular, the circle at the bottom-center represents the overall attraction exerted by

the goal. Above the circle the variance of that attraction is reported and under the circle the attraction vector is broken down into a module and an angle. In the circle on the right the single attraction exerted by each landmark is drawn. Each landmark has a number associated with it given by the value of the sigmoid function applied on its reliability measure. The arrows at the top-center of the figure represent the motion commands given to the robot.
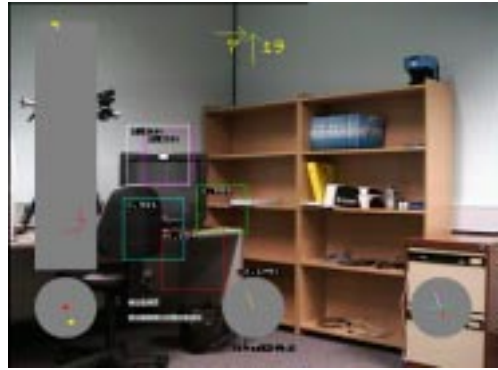

Figure 4: A frame taken by a real navigation task

Vector $\vec{V}$ represents the next movement with the module and direction relative to the actual robot position. The system dynamical model is therefore given by:

$$\begin{cases} x(k+1) = x(k) + V_x(x(k), y(k)) \\ y(k+1) = y(k) + V_y(x(k), y(k)) \end{cases} \qquad (5)$$

where $x(k)$ and $y(k)$ represent the coordinates of robot at step k; $V_x(x(k), y(k))$ and $V_y(x(k), y(k))$ the displacements computed at step k following equation 4. Those displacements are related to the position at step k given by $(x(k), y(k))$. Lastly, $x(k+1)$ and $y(k+1)$ represent the new positions the robot will move to. Clearly, an important equilibrium point (x^*, y^*) for the system is given by the coordinates of the goal position.

The navigation vector computed in equation 4 can be considered as the overall attraction exerted by the goal position from that place.

4 The guidance principle

There is evidence concerning the existence of a visual potential field around a goal position when robots are visually guided (Bianco et al., 1997; Gaussier et al., 1998; Cassinis et al., 1998; Bianco et al., 1999; Bianco and Zelinsky, 1999).

The nature of the area of attraction is intimately related to the existence of a *navigation field* represented by the navigation vectors from the points being considered. An example of a navigation vector field is represented by figure 5. The goal (represented by a small circle) seems to be located within a ba
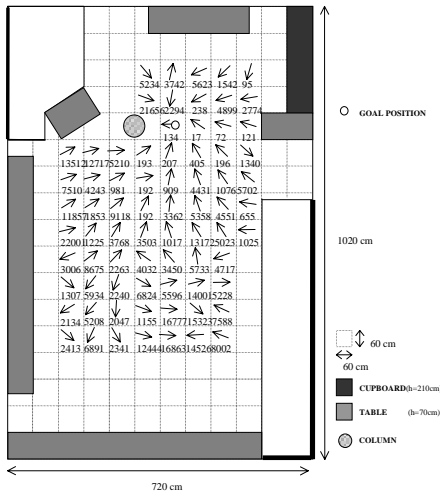
Figure 5: An example of a navigation field: directions and modules (numbers)

A key point for the comprehension of the connection links between the landmark learning phase and the navigation phase is the analysis of the navigation vector field. Therefore, we are strongly motivated to study these concepts in some detail.

Formally speaking, a vector field in two dimensions is a function that assigns to each point (x, y) of the xy-plane a two-dimensional vector $\vec{V}(x, y)$ usually represented by its two components:

$$\vec{V}(x, y) = [V_x(x, y) \ V_y(x, y)] \qquad (6)$$

where $V_x(x, y)$ is the x-component and $V_y(x, y)$ is the y-component. Note that in some cases the vector field is only defined for a region of the xy-plane.

A type of vector field arising in a number of disciplines is the *conservative* vector field. This is defined as one of which the integral computed on a

closed path is zero, i.e. the vector field $\vec{V}(x, y)$ is conservative if:

$$\oint_c \vec{V}(x, y) \circ d\vec{r} = 0 \qquad (7)$$

for any closed path c contained in the field of $\vec{V}$; $d\vec{r}$ is the infinitesimal direction of motion. Such a field can always be represented as the gradient of a scalar function defined by (Ross, 1995):

$$U(x, y) = \int_{(0,0)}^{(x,y)} \vec{V}(X, Y) \circ d\vec{r} \qquad (8)$$

where the path of integration is arbitrary. The scalar function U is referred to as the *potential* of the conservative force $\vec{V}$ in question. If the function $U(x, y)$ is known then the vector field can be determined from the relation:

$$\vec{V}(x, y) = \vec{\nabla} U(x, y) \qquad (9)$$

A non-conservative field is one in which the circuitation is non-null: the calculation of U depends on the path followed. In other words, U is not determined entirely by the extreme points.

All the considerations can be applied to the visual homing. Assuming that the goal position is located at the minimum of the potential basin, equation 9 is slightly modified with the following (Latombe, 1991; Khatib, 1986):

$$\vec{V} = [V_x \ V_y] = -\left[\frac{\partial U(x, y)}{\partial x} \ \frac{\partial U(x, y)}{\partial y} \right] \qquad (10)$$

If the field is conservative, the scalar product introduced in equation 8 can be further simplified by following a *particular* curve c (Ross, 1995):

$$U(x, y) = -\int_{p_x}^{x} V_x(X, p_y) dX - \int_{p_y}^{y} V_y(x, Y) dY \qquad (11)$$

where $U(x, y)$ is the potential function and the path of integration is along the horizontal line segment from the reference point (p_x, p_y) to the vertical line through (x, y) and then along the vertical line segment to (x, y).

It can be taken advantage of this method of computing the potential function by allowing as the reference point the coordinates of the goal position. Every other point is thus referred to in terms of potential in reference to the goal position.

If the field is not conservative then the integration detailed in equation 8 can lead to an infinite numbers of results depending on the curve c.

A practical application of equation 7 to state if the field is conservative needs to be found. To this extent, let's suppose that V_x and V_y are smooth and continuously differentiable and that the vector field is defined on a connected set. Under these hypothesis, a necessary and sufficient condition for the unique integration of the vector field is that the following relation (*Cauchy-Riemann*) holds (Strang, 1986):

$$\frac{\partial V_x(x,y)}{\partial y} = \frac{\partial V_y(x,y)}{\partial x} \qquad (12)$$

In other terms:

$$\frac{\partial V_x}{\partial y} - \frac{\partial V_y}{\partial x} = 0 \qquad (13)$$

The first member of equation 13 can be a measure of the level of *conservativeness* of the vector field.

4.1 Robustness of the visual potential function

In order to take advantage of the discussion presented so far and supposing that all the necessary hypotheses hold, the dynamic system presented in equation 5 can be considered continuous-time with the following (leaving out the vector notations):

$$\dot{x}(t) = V(x(t)) \qquad (14)$$

where x represent the generic coordinates and an equilibrium point x^* is located at the goal position.

Several important considerations for the stability of the system can be expressed focusing attention on its properties. In particular, when a dynamic system can be represented by $\dot{x} = f(x)$ with a fixed point x^*, and it is possible to find a *Liapunov function*, i.e. a continuously differentiable, real-valued function $U(x)$ with the following properties (Strogatz, 1994):

1. $U(x) > 0$ for all $x \neq x^*$ and $U(x^*) = 0$

2. $\dot{U} < 0$ for all $x \neq x^*$ (all trajectories flow *downhill* toward x^*)

then x^* is globally stable: for all initial conditions $x(t) \to x^*$ as $t \to \infty$.

The system depicted in equation 14 is of type $\dot{x} = f(x)$ but, unfortunately, there is no systematic way to construct Liapunov functions. In our case, a Liapunov function can be constructed by integrating the right-hand side of the system equation 14 (Luenberger, 1979). This automatically leads us to introduce the visual potential function as a good candidate for analyzing the overall stability of the system.

If the visual potential function has a basin of attraction with the minimum located at the goal position then the above introduced theory states that homing is intrinsically stable, at least starting navigating from within the convergent region of the environment.
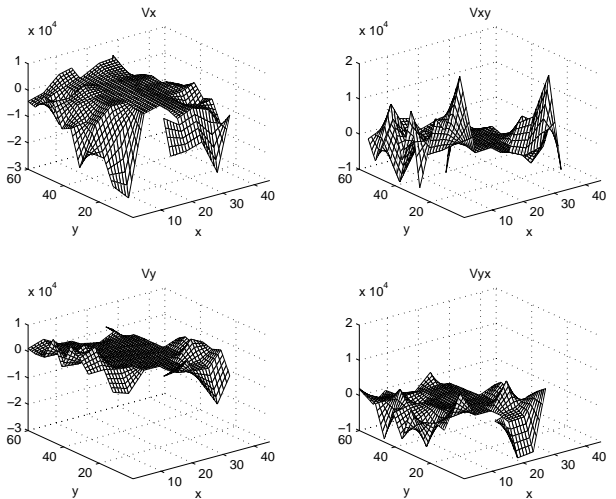

Figure 6: An example of V_x and V_y and their cross derivatives

5 Tests

As previously explained, tests have been performed both to measure how TBL affects the conservativeness of the navigation field and to calculate the region of convergence for the overall system.

The collection of the whole set of vectors (see equation 6) is performed firstly placing the robot in a known position of the environment and then applying the method detailed in equation 4. The iteration of the method over the whole environment and the collection of every displacement vector produces a vector field, as previously exemplified by figure 5. Each cell is approximately as big as the base of the robot.

Referring to equation 13 the partial derivatives of V_x and V_y must be computed. Figure 6 plots the
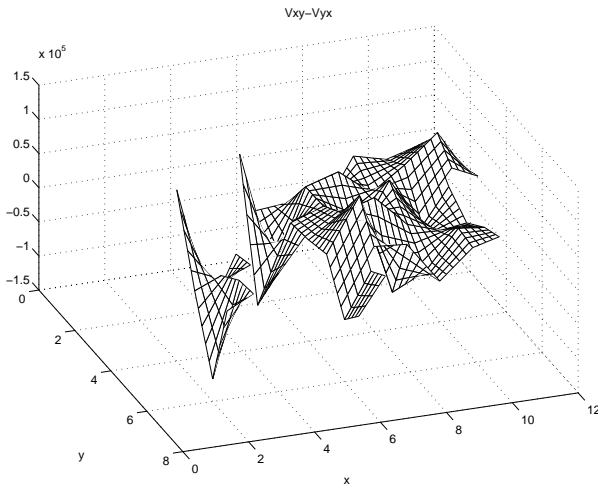
Figure 7: Conservativeness of a vector field computed with a TBL threshold of 0 and landmarks sized 6

components V_x and V_y and their cross derivatives $\frac{\partial V_x}{\partial y}$ and $\frac{\partial V_y}{\partial x}$ taken by a real test.

The conservativeness of the field computed with a threshold set to 0 and landmarks sized 6 is shown in figure 7. Only small regions of the whole area roughly satisfy the constraint. A small threshold for TBL can dramatically change the situation. In figure 8 the amount of conservativeness for each point is plotted.
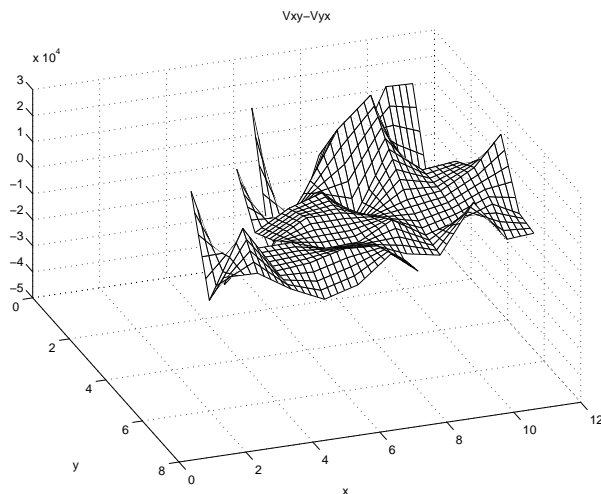
Figure 8: Conservativeness of a vector field computed with a TBL threshold of 0.10 and landmarks sized 6

A key consideration is concerned with the scale

along z: it is about one order of magnitude less than the one reported in figure 7. A trend toward a conservative field is thus becoming evident.

The situation obtained with a threshold of TBL set to 0.20 has been reported in figure 9. A large area of the environment has a measure of conservativeness that roughly equals 0.
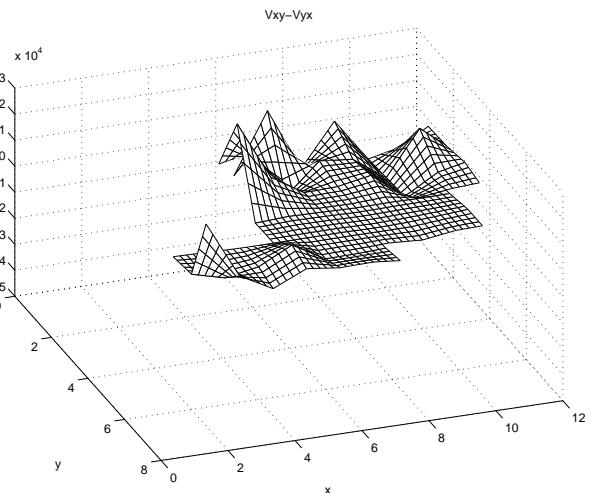

Figure 9: Conservativeness of a vector field computed with a TBL threshold of 0.20 and landmarks sized 6

Similar considerations can be expressed dealing with a different landmark size. For example, figure 10 shows the case where the TBL threshold is 0.20 and landmarks have a size of 4. The *template* of the graph is the same as before. Therefore, with a good choice of threshold the field becomes conservative regardless of the size of the landmarks.

5.1 Computation of the visual potential field

The computation of the visual potential field must be performed only on those areas of the environment which are conservative. From the results of the tests only two cases can be considered: when TBL threshold is set at 0.20 and landmarks have a size of 6 or 4. Starting with the former and following the method detailed in the previous section, the visual potential function is shown in figure 11.

The goal position is located in $(4, 5)$ and it represents the *reference point* for equation 11.

The shape of the potential function tends to produce a minimum around the goal (see figure 12).
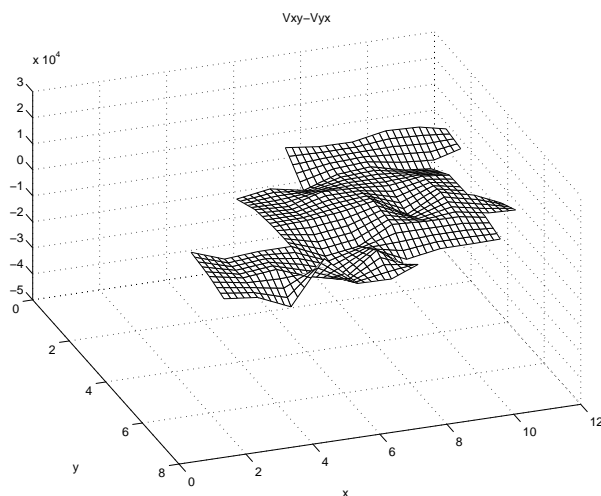
Figure 10: Conservativeness of a vector field computed with a TBL threshold of 0.20 and landmarks sized 4

Figure 11: Potential function computed with a TBL threshold set to 0.20 and landmarks sized 6

In addition, roughly speaking, the basin of attraction of the goal is the whole environment, i.e. apart from some cases, all the starting points lead to the goal. To this extent, consider the differences in the potential field showed in figure 14 where the TBL threshold is 0.20 but the landmark size is 4.

There are two important differences: the first concerns the basin of attraction and the second is concerned with the depth of the minimum in the goal position.

The basin of attraction determines how far a goal position can be *felt*. In other words, if the robot starts navigating within the basin of attraction then it reaches the goal position. Outside the basin the robot could lead to other (false) goals. The visual potential function reported in figure 11 possesses a larger basin of attraction than the one reported in figure 14 which influences the robot only when the robot is close to the goal.

Intriguingly enough, this has strong analogies with the biological results reported in (Cartwright and Collett, 1987). The authors discussed the area of attraction of the goal (namely, *the catchment area*) considering the size of landmarks surrounding it. Large landmarks determine larger catchment areas than smaller landmarks. Furthermore, larger landmarks determine a coarse approach to the goal whereas smaller landmarks allow the insects to precisely pinpointing the goal position.

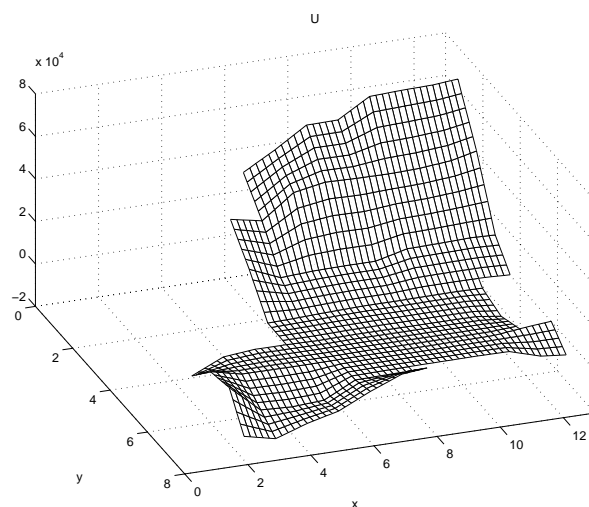To this extent, the visual potential function produced with landmarks sized 4 has a deeper minimum at the goal than the potential obtained with a size of 6 (see figure 13 compared to 12).

5.2 Issues on the visual potential as a Liapunov function

From the potential function previously plotted it can be easily understood why the system gets sometimes trapped into false goals or what can be the region of convergence for the main goal position.

This implicitly states that the system has not overall stability on the whole environment. Therefore, the visual potential function itself cannot be considered Liapunov compliant unless reducing its domain of application to a region around the goal position, starting from which the system converges (see e.g. figure 12).

6 Concluding remarks

This paper has presented the learning system of a biologically-inspired navigation method based on natural visual landmarks. The visual learning phase (TBL) affects the conservativeness of the navigation vector field thus allowing us to explain landmark navigation in terms of a potential field.

Conversely, the computation of the conservativeness of a navigation field can assess the reliability of the landmarks chosen and, therefore, measure the quality of the learning phase.
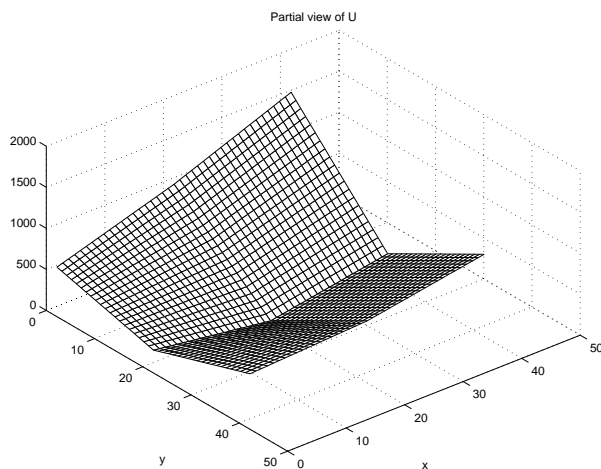
Figure 12: Potential function computed with a TBL threshold set to 0.20 and landmarks sized 6 magnificated 30 times around the goal
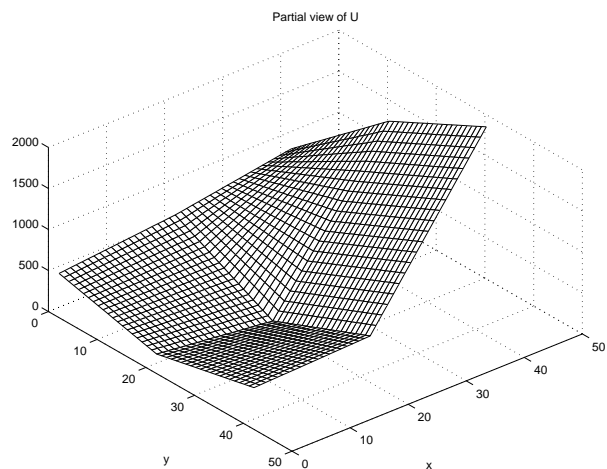

Figure 13: Potential function computed with a TBL threshold set to 0.20 and landmarks sized 4 magnificated 30 times around the goal

Lastly, the presence of a potential function around the goal allows us to apply classical control theories to assess the robustness of the overall navigation system. The idea of applying methods from vector analysis to navigation problems allows us to evaluate the performance of different models and can represent an important step for topological navigations.

References

Anandan, P. (1989). A computational framework and an algorithm for the measurement of visual motion. *International Journal of Computer Vision*, (2):283–310.

Bianco, G. (1998). *Biologically-inspired visual landmark learning and navigation for mobile robots*. PhD thesis, Department of Engineering for Automation, University of Brescia (Italy).

Bianco, G., Cassinis, R., Rizzi, A., and Scipioni, S. (1997). A proposal for a bee-inspired visual robot navigation. In *Proceedings of the First Workshop on Teleoperation and Robotics Applications in Science and Arts*, pages 123–130, Linz (Austria).

Bianco, G., Rizzi, A., Cassinis, R., and Adami, N. (1999). Guidance principle and robustness issues for a biologically-inspired visual homing.

In *Proceedings of the Third Workshop on Advanced Mobile Robots (EUROBOT '99)*, Zurich (Switzerland).

Bianco, G. and Zelinsky, A. (1999). Biologically-inspired visual landmark learning for mobile robots. In *Proceedings of the IEEE/RSJ International Conference on Intelligent Robots and Systems*, Kyongju (Korea).

Borenstein, J., Everett, H., and Feng, L. (1996). *Where am I? Sensors and Methods for Mobile Robot Positioning*. The University of Michigan.

Cartwright, B. and Collett, T. (1983). Landmark learning in bees. *Journal of Comparative Physiology*, A(151):521–543.

Cartwright, B. and Collett, T. (1987). Landmark maps for honeybees. *Biological Cybernetics*, (57):85–93.

Cassinis, R., Rizzi, A., Bianco, G., Adami, N., and Mosna, P. (1998). A biologically-inspired visual homing method for robots. In *Proceedings of seventh workshop of AI*IA on Cybernetic and Machine Learning*, Ferrara (Italy).

Cheng, K., Collett, T., Pickhard, A., and Wehner, R. (1987). The use of visual landmarks by honeybees: Bees weight landmarks according to their distance from the goal. *Journal of Comparative Physiology*, A(161):469–475.
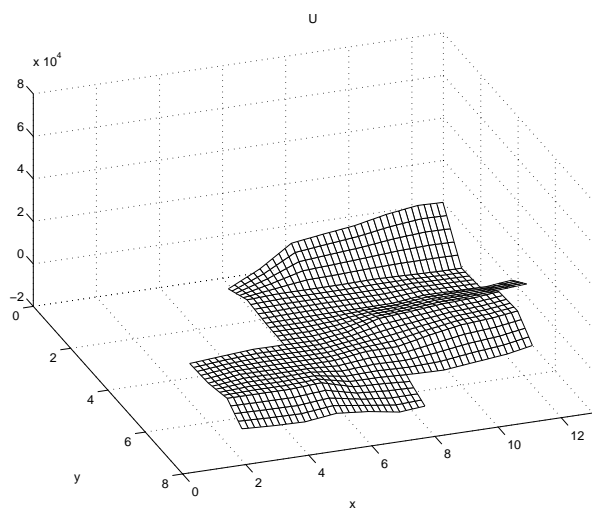
Figure 14: Potential function concerning the case with a TBL threshold set to 0.20 and landmarks sized 4

Collett, T. and Zeil, J. (1996). Flights of learning. *Journal of the American Psychologycal Society*, pages 149–155.

Gaussier, P., Joulain, C., and Banquet, J. (1998). Motivated animat navigation: a visually guided approach. In *Simulation of Adaptive Behavior*, Zurich (Switzerland).

Khatib, O. (1986). Real-time obstacle avoidance for manipulators and mobile robots. *Int. Journal of Robotics Research*, 4(1):90–98.

Latombe, J. (1991). *Robot motion planning*. Kluwer Academic Publisher, Boston/Dodrecht/London.

Lehrer, M. (1993). Why do bees turn back and look? *Journal of Comparative Physiology*, A(172):549–563.

Lehrer, M. (1997). Honeybees' visual spatial orientation at the feeding site. In Lehrer, M., editor, *Orientation and communications in arthropods*, pages 115–144. Birkhauser verlag, Basel/Switzerland.

Little, J. and Verri, A. (1989). Analysis of differential and matching methods for optical flow. In *Proceedings of the IEEE workshop on visual motion*, pages 173–180, Irvine, CA.

Luenberger, D. (1979). *Introduction to dynamic systems - theory, models, and applications.*

John Wiley and Sons, New York Chichester Brisbane Toronto.

Mori, T., Matsumoto, Y., Shibata, T., Inaba, M., and Inoue, H. (1995). Trackable attention point generation based on classification of correlation value distribution. In *JSME Annual Conference on Robotics and Mechatronics (ROBOMEC 95)*, pages 1076–1079, Kavasaki (Japan).

Ross, C. (1995). *Differential Equations An Introduction with Mathematica*. Springer-Verlag, New York Berlin Heidelberg London Paris Tokyo Hong Kong Barcelona Budapest.

Strang, G. (1986). *Introduction to Applied Mathematics*. Wensley-Cambridge Press.

Strogatz, S. (1994). *Nonlinear dynamics and chaos*. Addison-Wesley Publishing Company, New York.

Thrun, S. (1996). A bayesian approach to landmark discovery and active perception in mobile robot navigation. Technical report, School of Computer Science Carnegie Mellon University.

Trullier, O., Wiener, S., Berthoz, A., and Meyer, J. (1997). Biologically based artificial navigation systems: Review and prospects. *Progress in Neurobiology*, 51:483–544.

Wehner, R. (1992). Arthropods. In Papi, F., editor, *Animal Homing*, pages 45–144. Chapman and Hall, London.

Zeil, J., Kelber, A., and Voss, R. (1996). Structure and function of learning flights in bees and wasps. *Journal of Experimental Biology*, 199:245–252.
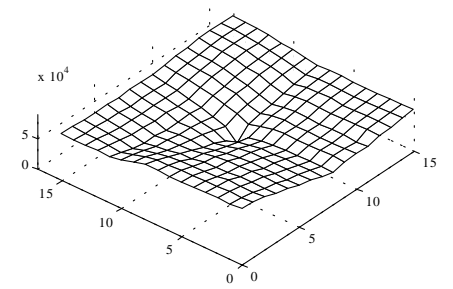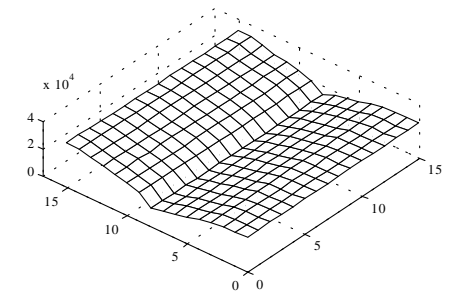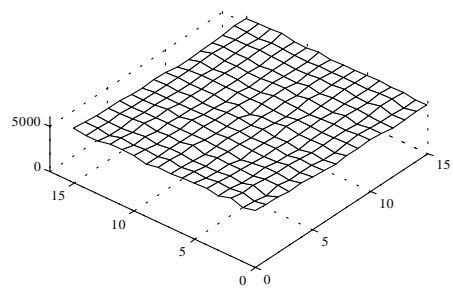
Figure 15: Examples of distortion matrices which have been computed in the neighborhood of the templates (boxes in the pictures).
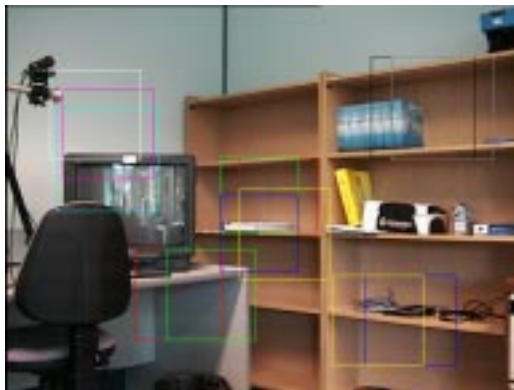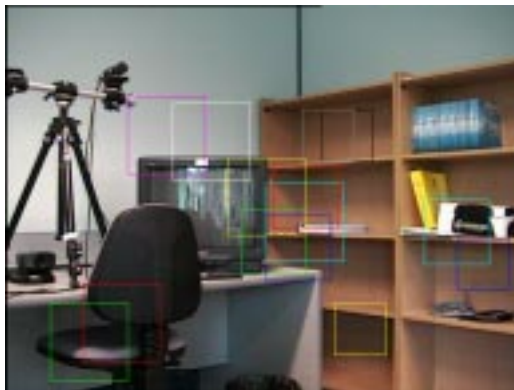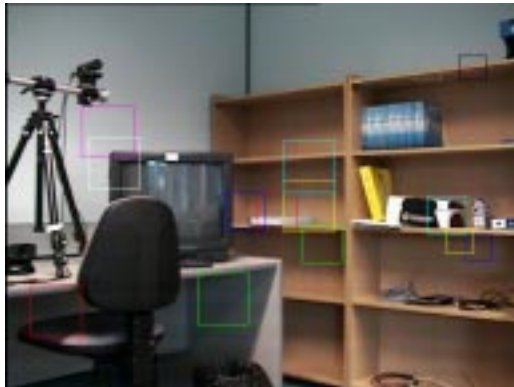
Figure 16: Different choices of landmarks for different landmark sizes

Figure 17: Two pictures taken from a TBL phase: the numbers associated with each landmark represent r_l in different times